Bull. Mater. Sci., Vol. 37, No. 3, May 2014, pp. 527–532. © Indian Academy of Sciences.

Structural verification and optical characterization of SiO_2–Au–Cu_2O nanoparticles

HOSSEIN REZVANI NIKABADI, NASSER SHAHTAHMASEBI, MAHMOOD REZAEE ROKN-ABADI, MASOUD KARIMIPOUR[1,*] and M M BAGHERI MOHAGHEGHI[2]

Physics Department, Ferdowsi University of Mashhad, Mashhad, Iran
[1]Department of Physics, Vali-E-Asr University of Rafsanjan, 77139-36417 Rafsanjan, Iran
[2]School of Physics, Damghan University, Damghan, Iran

MS received 31 January 2013; revised 24 February 2013

Abstract. **In this paper, SiO_2–Au–Cu_2O core/shell/shell nanoparticles were synthesized by reducing gold chloride on 3-amino-propyl-triethoxysilane molecules attached silica nanoparticle cores for several stages. Cu_2O nanoparticles were synthesized readily with the size of 4–5 nm using a simple route of sol–gel method. Then, they were clung to the surface of Au seeds. The morphology of the resultant particles was studied using transmission electron microscopy (TEM) and scanning electron microscopy (SEM). Transmission electron microscopy images demonstrate growth of monodispersed gold seeds and Cu_2O nanoparticles in narrow size up to 10 nm and 5 nm, respectively. The presence of gold and Cu_2O coating was confirmed by X-ray diffraction, Fourier transform infrared spectroscopy and UV–Vis spectroscopy. Absorption spectroscopy shows considerably 40 nm blue shift in absorption edge for SiO_2–Au–Cu_2O nanostructure rather than SiO_2–Au core/shell nanoparticles.**

Keywords. **Plasmon; blue shift; SiO_2–Au–Cu_2O core/shell/shell; sol–gel; APTES molecules.**

1. Introduction

Metallic nanostructured materials have attracted a lot of attention due to their novel properties in light harvesting and photo manipulating and their application in photonic components (Costi *et al* 2010). On the other hand, comparing to those of nanowires and nanorods, metal–semiconductor core/shell materials show relatively strong plasmonic tunability dependent on the size and morphology of inner and outer shell. Furthermore, metallic nanoshells, spherical nanoparticles composed of a dielectric core and a concentric metal shell, are nanoparticles whose plasmon resonant energies are particularly sensitive to geometry (Oldenburg *et al* 1998; Xia *et al* 2005). Plasmonic resonance energy can be tuned due to hybridization of one nanoshell encapsulated within another nanoshell, also known as a 'nanomatryushka' geometry (Prodan *et al* 2003; Radloff *et al* 2004). SiO_2–Au core/shell structures have been extensively studied (Enustun *et al* 1963; Hache *et al* 1988; Bigot *et al* 1995; Liz-Marzan *et al* 1996; Perener *et al* 1997; Westcott *et al* 1998; Moroz 1999, 2000; Zhang *et al* 2000). Also, Au–Cu_2O (Kandpal *et al* 2007) has shown further tunable property and new synergistic properties that arise from the interactions between metal and semiconductor components.

Recent developments in colloidal nanoparticle synthesis has resulted in precise preparation of a variety of hybrid metal–semiconductor nanostructures, such as metal-decorated anisotropic semiconductor nanoparticles, nanoparticle heterodimers and core–shell heterostructured nanoparticles with various compositional combinations and arrangements. Many spectacular phenomena were observed from the interactions between the confined metal and semiconductor components have been observed in these hybrid heteronanostructures. It has been reported that the presence of metallic ingredients may significantly increase the photocatalytic and light-harvesting efficiencies for solar cell applications by improving the charge separation at the semiconductor–metal interfaces and/or by enhancing the light absorption (Zhang *et al* 2011). Although, there are many literatures on the role of geometry and size on the tenability of plasmonic energy, there are so far a few reports on the optical properties of heterostructured dielectric/metal/semiconductor comprising two different semiconductors. In this study, we describe the preparation of SiO_2–Au–Cu_2O core/shell/shell using combination of sol–gel and chemical reduction methods. Afterwards, characterization of the resultant structure has been performed by means of X-ray diffraction (XRD), transmission electron microscopy,

*Author for correspondence (masoud.karimipour@gmail.com)

scanning electron microscopy (SEM), Fourier transform infrared (FT–IR) spectroscopy and ultraviolet–visible (UV–Vis) spectroscopy.

2. Experimental

2.1 *Materials*

All materials were purchased from the indicated suppliers and used without further purification: tetraethylorthosilicate, tetrakishydroxy methyl phosphonium chloride (THPC), 3-aminopropyltriethoxysilane, sodium hydroxide, ammonium hydroxide, formaldehyde and hydrogen tetrachloroaurate (III) (all from Merck Co.). Similarly, all solvents were used as-received from the indicated suppliers: HPLC grade water, absolute ethanol (Merck Co.), copper (II) nitrate trihydrate, citric acid and ethylene glycol.

2.2 *Characterization methods*

The crystalline structure of silica core and core/shell SiO_2–Au nanoparticles were recorded with the help of D8-Advance Bruker X-ray diffractometer using CuKα radiation ($\lambda = 1{\cdot}54056$ Å) in the range of $2\theta = 20$–$80°$. SEM images have been obtained by scanning electron microscopy model LEO 1450 VP system. To collect the TEM images, we used a LEO912 AB electron microscope operating at a bias voltage of 200 kV. Sample preparation involved deposition of the nanoparticles dispersed in water onto a 200 mesh copper grid. The grid was then set aside to allow for evaporation of any residual water before analysis. FT–IR data were collected using an AVATAR-370-FT–IR Thermonicolet spectrometer using two separate procedures. Sample was unpacked into a tablet shape and put onto a polished silicon wafer before analysis. UV–Vis spectra were collected using a UVD-2950.LABOMED UV-Visible spectrometer over the range of 400–900 nm. All samples were dispersed in water and into a quartz cell for analysis.

2.3 *Preparation of silica nanoparticles*

0·2 mL of ammonia (30% NH_3 as NH_4OH assay) was added to 50 mL of absolute ethanol. The mixture was stirred vigorously, and a subsequent aliquot (1 mL, 4·2 mmol) of $Si(OC_2H_5)_4$ (TEOS) was added drop-wise. For the concentrations employed here, the induction period was ~ 1·5 h as judged by the change of the solution from clear to opaque white. The concentration of the resultant silica nanoparticles was 7×10^{12} particles/mL. Analysis by TEM indicated that the silica nanoparticles were spherical in shape with 100 nm diameter.

2.4 *Functionalization of silica nanoparticles surface with APTES*

The surface of silica nanoparticles were functionalized by grafting them with 12 mM APTES in volume ratio of 3 : 7 under constant heating and vigorous stirring at 77 °C for 3 h to give a terminal amine group on their surface. To reach the best conditions, APTES was used again with molar excess. Because APTES exposes an amine group with an available electron lone pair that can coordinate to achieve a complete surface functionalization. Then, the amine-grafted silica particles were cooled to room temperature and washed with at least 2 cycles of centrifugation and re-dispersion in absolute ethanol and distilled water at 10,000 rpm for 15 min each to remove residual reactants before re-suspending them in 1 mL of water for every 0·3 g of silica used for surface functionalization with amine.

2.5 *Preparation of colloidal gold nanoparticles*

0·5 mL of NaOH 1 M was added to a 45 mL aliquot of HPLC grade water and 1 mL of THPC solution (prepared by adding 12 μL (0·067 mmol) of 80% THPC in water to 1 mL of HPLC grade water). The reaction mixture was stirred for 5 min with a strong vortex in the reaction flask. After the allotted time, 1 mL (27 mmol) of 1% $HAuCl_4$ in water was added quickly to the stirred solution, which was stirred further for 30 min. At this time, colour of the solution changed very quickly from colourless to dark reddish yellow, which we call 'THPC gold nanoparticles'. Although, size of THPC gold nanoparticles can be varied, our gold seeds were consistently 2–4 nm in diameter. The solution of THPC gold seeds was placed in the refrigerator for at least 3 days before further use. Dried samples of the gold nanoparticles were dark brown in colour.

2.6 *Attachment of colloidal gold nanoparticles to APTES functionalized silica cores*

An aliquot of APTES-functionalized silica nanoparticles dispersed in ethanol (6·7 mL, $2{\cdot}4 \times 10^{13}$ particles/mL) was placed in a centrifuge tube along with an excess of gold nanoparticles (5 mL of gold colloidal solution, $3{\cdot}5 \times 10^{14}$ particles/mL). The centrifuge tube was shaken gently for a couple of minutes and then allowed to sit for 3 h. The mixture was then centrifuged at 2000 revolutions/min and a red-coloured pellet was observed to settle at the bottom of the tube. After drying, a red-coloured pellet was left, which was re-dispersed and sonicated in HPLC grade water. The purified silica/APTES/gold nanoparticles were then re-dispersed in 5 mL of HPLC grade water and used as described in the following subsection. The gold metal has very little affinity for silica, and it does not form the passivating oxide film in solution.

Therefore, silane coupling agent is used as surface primer. The strong chemical affinity of primary amine for gold, drives chemisorptions of the colloids in the case of APTES (Kandpal *et al* 2007). Consequently, the interaction between the amines and the negatively charged THPC gold nanoparticles might be electrostatic rather than coordinative in nature (Westcott *et al* 1998).

2.7 *Growth of gold nanoshell*

To grow the gold nano-shell on the silica/APTES/gold nanoparticles, we first had to prepare a suitable solution containing a reducible gold salt. In a reaction flask, we dissolved 25 mg (0·18 mmol) of potassium carbonate (K_2CO_3) in 100 mL of HPLC grade water. After 10 min of stirring, 1·5 mL (20 mmol) solution of 1% $HAuCl_4$ in water was added. The solution initially appeared transparent yellow and slowly became colourless over the course of 30 min, then we injected 200 μL of the solution containing silica/APTES/gold nanoparticles to a vigorously stirred 4 mL aliquot of the colourless solution. Afterwards, we added a 10 μL (0·36 mmol) aliquot of formaldehyde. Over the course of 2–4 min, the solution changed from colourless to blue, which is characteristic of nanoshell formation. The nanoshells were centrifuged and re-dispersed in HPLC grade water until use.

2.8 *Preparation of Cu_2O nanoparticles via sol–gel method*

To prepare starting solution, 0·003 mol of $Cu(NO_3)_2 \cdot 3H_2O$ was dissolved in solvent containing equivalent 15 ml of absolute ethanol and deionized water and stirred for 30 min. Thereafter, 0·003 mol of both citric acid and ethylene glycol were added to the starting solution and stirred using magnetic stirrer at 40 °C for 1 h. The prepared sol was then refluxed at 100 °C for 6 h.

2.9 *Growth of Cu_2O shell on SiO_2–Au core/shell*

The prepared SiO_2–Au nanoparticles were dispersed in 5 ml of HPLC water and sonicated for 30 min. Then the resultant liquid was added to the sol containing Cu_2O particles which was explained in §2.8. Thereafter, 0·5 mol of $NaBH_4$ was added drop-wise to the resultant solution under stirring. The final solution was stirred for 90 min and then centrifuged at a speed of 9000 rpm for 30 min. The resultant powder was subtracted from the liquid and washed several times and dried at room temperature.

3. Results and discussion

3.1 *XRD, SEM and TEM characterizations*

XRD patterns of silica, SiO_2–Au and SiO_2–Au–Cu_2O core/shell/shell are depicted in figures 1(a–c), respectively. Figure 1(a) is related to the silica nanoparticle which shows the amorphous structure. XRD pattern of SiO_2–Au nano core/shell is shown in figure 1(b). The

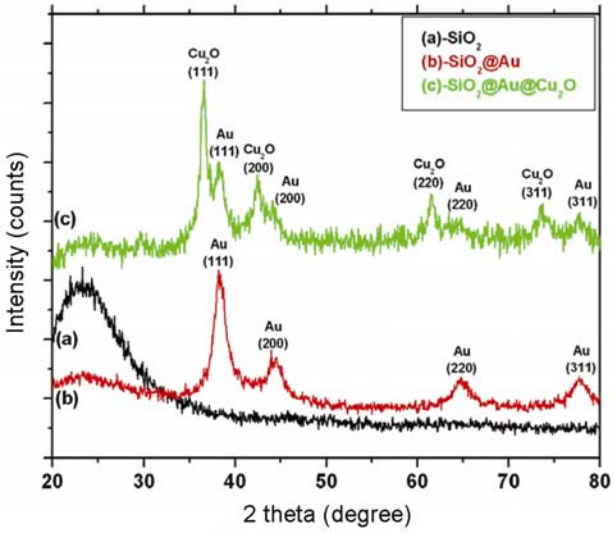

Figure 1. XRD patterns of (**a**) pure silica nanoparticles, (**b**) SiO_2–Au core/shell nanoparticles and (**c**) SiO_2–Au–Cu_2O core/shell/shell nanoparticles.

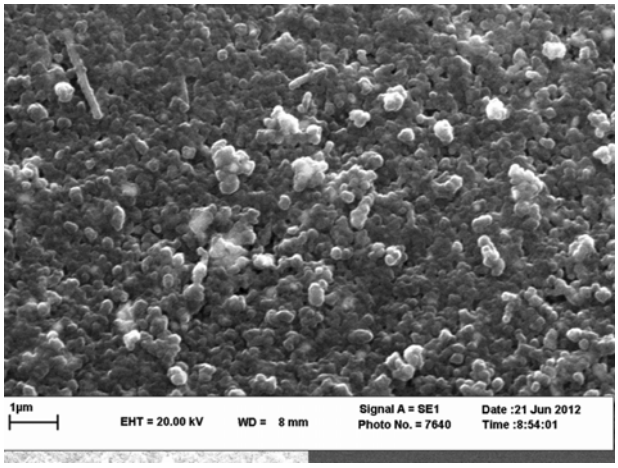

Figure 2. SEM images of SiO_2–Au–Cu_2O core/shell/shell nanoparticles.

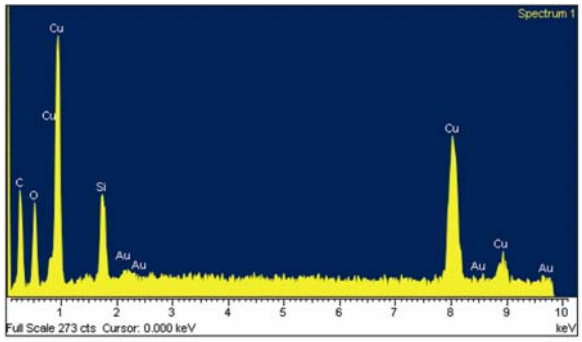

Figure 3. EDX spectra of SiO_2–Au–Cu_2O core/shell/shell nanoparticles.

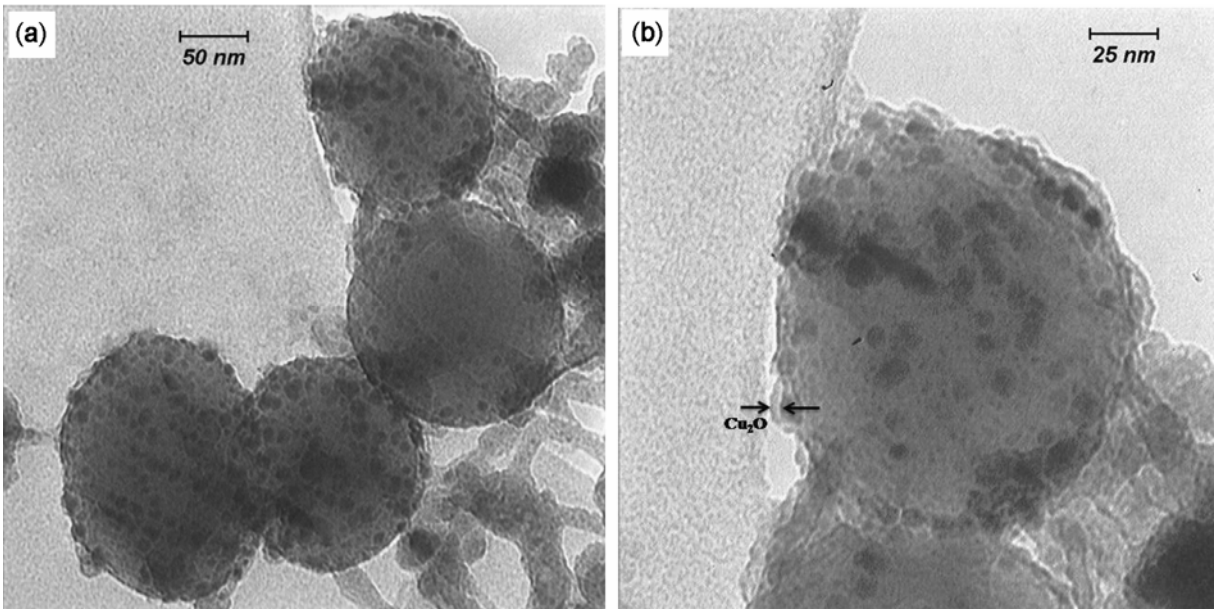

Figure 4. TEM images of SiO_2–Au–Cu_2O core/shell/shell nanoparticles.

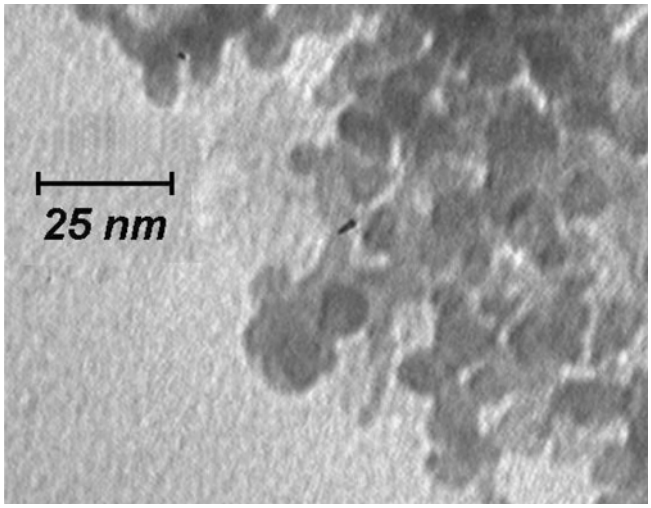

Figure 5. TEM image of colloidal gold nanoparticles.

crystalline structure of SiO_2–Au nanoparticles are face-centred-cubic (*fcc*) with the dominant crystal growth planes of (111) and displays peaks for both silica and gold. Cu_2O shell has been formed on top of Au shell (figure 1(c)) which has polycrystalline cubic structure with the preferential growth plane of (111). The appearance of comparatively sharp (200) and (220) peaks in the diffraction pattern show that the Cu_2O is well crystallized.

SEM image of resultant powder (figure 2) shows that the structure has been formed uniformly both in size distribution and material growth. There is no other contrast, from which one could conclude the formation of other individual structures like Cu_2O nanoparticles or Au-mixed particles. To qualitatively discuss the material specification in the structure, EDX spectra was prepared (figure 3). It reveals that Si, Au and Cu are present in the structure. The rather disproportional amount of Si and Au comes from two main reasons. First, EDX technique is rather weak in quantitative prediction of elemental specification. Second, X-rays coming out from the SiO_2 core and Au shell are reabsorbed or scattered by Cu_2O shell. Thus, the Cu peak in the spectra is significantly higher than Si.

TEM images (figure 4) verify the formation of SiO_2–Au–Cu_2O core/shell/shell structure. It clearly shows the contrast of electron density of Au intermediated layer (dark in the image) and SiO_2 and Cu_2O surroundings. It can be observed that SiO_2 particle size is roughly 80 nm and Au shell may be estimated to be about 10–12 nm (figure 5). Moreover, Cu_2O layer thickness is < 5 nm.

3.2 FT–IR *analysis*

The results of Fourier transform infrared spectroscopy are shown in figure 6. It contains FT–IR spectrum of silica, SiO_2–Au and SiO_2–Au–Cu_2O nanoparticles. For SiO_2, SiO_2–Au and SiO_2–Au–Cu_2O nanoparticles, peak at 1104 cm^{-1} can be assigned to Si–O–Si bond and peak at 945 cm^{-1} can be attributed to Si–OH, peak at 3429 cm^{-1} is assigned to N–H bond, which shows the presence of amine-grafted silica particles in SiO_2–Au nanoparticles. The weak absorption bands between 1300 and 1700 cm^{-1} are mainly ascribed to the chemisorbed and/or physisorbed H_2O and CO_2 molecules on the surface of nanostructured Cu_2O. The peak at ~ 1638 cm^{-1} was due to the bending vibration of water, which is formed after Cu_2O

deposition was removed. Also, the appearance of new absorption peak at 615 cm^{-1} corresponding to the infrared active mode of Cu_2O was seen (Beganskienè *et al* 2004; Mageshwari *et al* 2012). After coating these particles with gold and Cu_2O, intensities of Si–O–Si and Si–OH peaks reduced significantly.

3.3 *UV-Vis analysis*

Figure 7 shows absorption spectra of Au, SiO_2–Au, Cu_2O and the multi-shell SiO_2–Au–Cu_2O structures. Observation

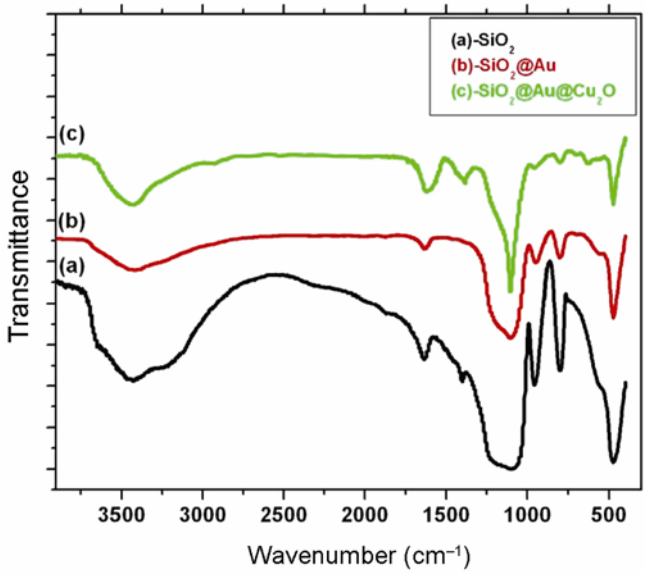

Figure 6. FT–IR spectra of (a) pure silica nanoparticles, (b) SiO_2–Au core/shell nanoparticles and (c) SiO_2–Au–Cu_2O core/shell/shell nanoparticles.

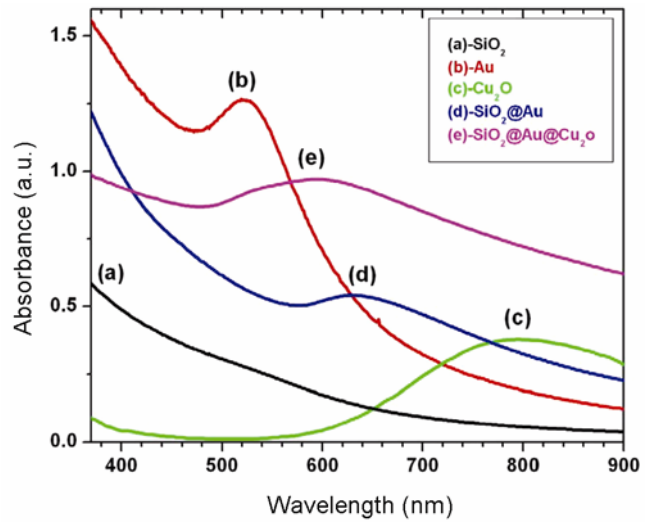

Figure 7. Optical absorption (UV–Vis) of silica, Au, Cu_2O, SiO_2–Au core/shell nanoparticles and SiO_2–Au–Cu_2O core/shell/shell nanoparticles.

of absorption plasmonic peaks of Au at 520 nm, SiO_2–Au at 640 nm and Cu_2O at 800 nm are consistent with other reports (Zhang *et al* 2011). This confirms also the accuracy of the preparation methods which are applied to prepare the final structure of SiO_2–Au–Cu_2O.

Moreover, the absorption spectrum of SiO_2–Au–Cu_2O structure shows a broad peak centred at a wavelength of 590 nm. These show a blue shift compared to SiO_2–Au structure. It can be due to the new boundary condition for Au electrons which neighbour the outermost of Au shell. The proximity of Cu_2O shell confines the Au electron, so that according to Mai theory (Boardman 1982), electron confinement in metals results in a decrease in absorption intensity and broadening of the peak. It can be seen that the peak spans from Au absorption peak to SiO_2–Au absorption peak.

It is worth noticing that when SiO_2–Au absorption is measured, the measurement takes place in a liquid buffer. When Au neighbours the liquid (with mean refractive index of 1·6), the absorption peak is at 640 nm. But, replacing it with Cu_2O (refractive index: 2·85), one should take into account the change in refractive index of the environment (Zhang *et al* 2011). Based on Mai theory, when the refractive index of environment on the surface of metal increases, a red shift will happen. But, this red shift is just few nanometers. On the other hand, according to hydrodynamic theory of plasmon–polaritons (Boardman 1982), structural confinement of Au electrons causes an interaction of plasmonic waves from surface electrons of both sides of Au. Thus, they are more bounded and need more energy to be excited. So a significant blue shift will take place that outweigh the red shift.

4. Conclusions

SiO_2–Au–Cu_2O core/shell/shell nanoparticles were synthesized by reducing gold chloride on APTES attached silica nanoparticle cores for several stages. Cu_2O nanoparticles were synthesized readily with size of 4–5 nm using a simple route of sol–gel method. Then, they were clung to the surface of Au seeds. The morphology of these particles was studied using TEM and SEM. TEM images demonstrate growth of monodispersed gold seeds and Cu_2O nanoparticles in narrow size up to 10 nm and 5 nm, respectively. The presence of gold and Cu_2O coatings were confirmed by XRD, FT–IR and UV/Vis spectroscopy. Absorption spectroscopy shows a blue shift for SiO_2–Au–Cu_2O heterostructure rather than SiO_2–Au core/shell nanoparticles. It is due to the surface plasmon confinement. Moreover, the peak is broadened and confirms that boundary conditions have great effect on both plasmonic resonance frequency and their life-time. This can be interpreted as a promising candidate for light scattering in the range of 500–700 nm for solar cell applications.

References

Bigot J Y, Merle J C, Cregut O and Daunois A 1995 *Phys. Rev. Lett.* **75** 4702

Beganskienè A, Sirutkaitis V, Kurtinaitieeè M, Juškènas R and Kareiva A 2004 *Mater. Sci.* **10** 287

Boardman A 1982 *Electromagnetic surface modes: hydrodynamic theory of plasmon–polaritons on plane surfaces* (S. Chichester: John Wiley)

Costi R, Saunders A E and Banin U 2010 *Angew. Chem. Int. Ed. Engl.* **49** 4878

Enustun B V and Turkevich J J 1963 *Am. Chem. Soc.* **85** 3317

Hache F, Richard D, Flytzanis C and Kribig U 1988 *Appl. Phys.* **47** 347

Kandpal D, Kalele S and Kulkarnl S K 2007 *Pramana* **69** 277

Liz-Marzan L M, Giersig M and Mulvaney P 1996 *Langmuir* **12** 4329

Moroz A 1999 *Phys. Rev. Lett.* **83** 5274

Moroz A 2000 *Europhys. Lett.* **50** 466

Mageshwari K and Sathyamoorthy R 2012 *Appl. Nanosci.* 1

Oldenburg S J, Averitt R D, Westcott S L and Halas N J 1998 *Chem. Phys. Lett.* **288** 243

Prodan E, Radloff C, Halas N J and Nordlander P 2003 *Science* **302** 419

Perener M, Bost P, Lemmer U, Plessem G V, Feldmann J, Becker U, Menig M, Schmitt M and Schmidt H 1997 *Phys. Rev. Lett.* **78** 2192

Radloff C and Halas N J 2004 *Nano Lett.* **4** 1323

Westcott S L, Oldenburg S J, Lee T R and Halas N J 1998 *Langmuir* **14** 5396

Xia Y and Halas N J 2005 *MRS Bulletin* **30** 338

Zhang W Y, Lei X Y, Wang Z L, Zheng D G, Tam W Y, Chang C T and Sheng P 2000 *Phys. Rev. Lett.* **84** 2853

Zhang L, Blom D A and Wang H 2011 *Chem. Mater.* **23** 4587

Zhang L and Wang H 2011 *ACS Nano.* **5** 3257